Ionogels at the water energy nexus for desalination powered by ultra low grade heat

Ionogels at the water energy nexus for desalination powered by ultra low grade heat

Christopher Olkis,[†] Hongsheng Dong,[‡] Stefano Brandani,[†] and Giulio Santori[*,†]

[†] *The University of Edinburgh, School of Engineering, Institute for Materials and Processes, Sanderson Building, The King's Buildings, Mayfield Road, EH9 3FB Edinburgh, UK*

[‡] *Thermochemistry Laboratory, Dalian Institute of Chemical Physics, Chinese Academy of Science, Liaoning Province Key Laboratory of Thermochemistry for Energy and Materials, Dalian National Laboratory for Clean Energy, Dalian 116023, China*

E-mail: G.Santori@ed.ac.uk

Abstract

Industrial processes emit enormous amounts of waste heat below 40 °C into the environment as it is cannot be used in other processes. Adsorption desalination can be driven by low grade heat, but has never been proven at temperatures below 40 °C as current adsorption materials require heat sources of 50-150 °C. Here, we present the first experimental study on adsorption desalination using a novel class of ionogel adsorption materials, which can be regenerated at 25 °C or a driving temperature difference of 5 °C. This outstanding property contrasts with the benchmarking silica gel, which requires heat sources of at least 50 °C. Ionogels are solid-state ionic

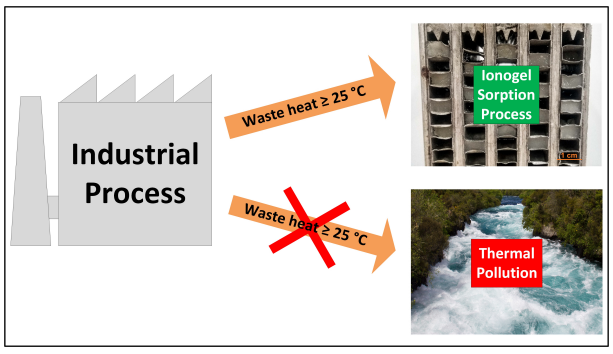

materials retaining the sorption properties of the constituent ionic liquid. Thermodynamic vapour-liquid equilibrium data of water sorption on commercial ionic liquids reveals 1-ethyl-3-methylimidazolium acetate as best fluid for this specific application. A full experimental characterisation of the material is performed from imaging at nano-scale to testing on a real adsorption desalinator. At 25 °C the material achieves a Specific Daily Water Production of 6.7 $kg_{water}/(kg_{ionogel}d)$ increasing to 17.5 $kg_{water}/(kg_{ionogel}d)$ at 45 °C outperforming silica gel by a factor of two.

Keywords: Adsorption desalination, heat transformer, ionic liquid, low-grade heat, experimental analysis

Introduction

Low-grade heat is a waste product from industrial processes, which is often discharged into the environment causing thermal pollution. Thermal pollution to water bodies can significantly harm aquatic environments[1,2] as most aquatic life has a limited temperature tolerance.[3]

More than two thirds of all primary energy is converted into waste heat with the majority arising below 100 °C.[4] In the United States alone, 4000 TWh/year of waste heat are emitted below 50 °C by industry and power plants,[5] which heavily depend on water resources for cooling.[6,7] These vast quantities of waste heat cause economic loss and thermal pollution as it is emitted into the environment, atmosphere, oceans and rivers.[8] Furthermore, during hot summers power plants in Europe and the United States often have to shut down because of the increase in river water temperature.[6] Global warming will further increase river water temperatures[6] reducing power plant productivity in the future.[9,10]

One of the largest, single sources of waste heat are power plant condensers. A 500 MW_{el} nuclear power plant can emit 1100 MW_{th} of waste heat at 26 °C.[11] However, to date no

thermal process can be driven by a waste heat source of 26 °C. Low grade heat can drive desalination processes, which require at least 50 °C as shown in Fig. 1 with the exception of the ionogel material presented in this study.

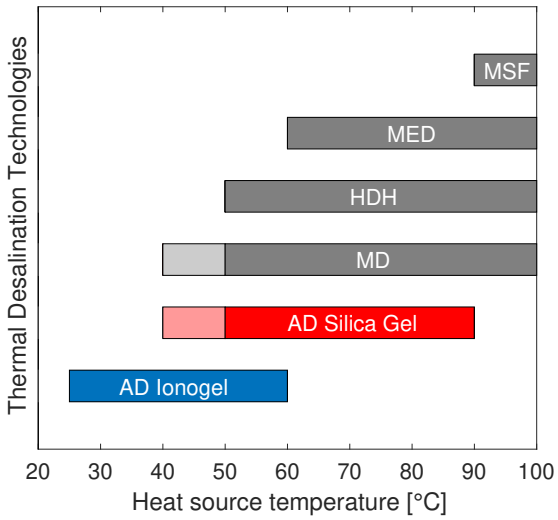

Figure 1: Comparison of thermal desalination technologies in terms of their heat source temperatures: MSF: Multi stage flash;[12] MED: Multi effect distillation;[13] HDH: Humidification dehumidification desalination;[14] MD: Membrane distillation;[15,16] AD: Adsorption desalination using silica gel[17,18] and ionogel.[19] Lighter colors indicate applicability at strongly reduced efficiency.

Waste heat can also be converted into electricity,[20,21] where Organic Rankine Cycle systems require heat sources of at least 80 °C.[22] In addition, osmotic heat engines[23] and reverse electrodialysis heat engines were developed[24,25] to generate electricity from low grade heat.[26] Both operate by combining reverse electrodialysis[27] or pressure retarded osmosis membranes[28] with a thermal desalination system including adsorption desalination.[29] Sorption desalinators[30] emerged from adsorption chillers[31,32] and can be driven by low-grade heat as low as 50 °C when silica gel is used.[18] However, silica gel provides half the performance when the heat source temperature is reduced from 80 °C to 50 °C.[33] Replacing silica gels with novel, advanced adsorption materials[34] promises enhanced performances at lower regeneration temperatures.[35,36]

Ionogels represent a novel class of hybrid sorption materials, where a solid support structure

is impregnated with an ionic liquid[37] while retaining its unique properties.[38,39] By definition, ionic liquids are organic salts with melting points below 100 °C featuring high ionic conductivity, negligible vapour pressure, high thermal stability and non-flammability.[38] Imidazolium ionic liquids are reported as some of the most important and most investigated types of ionic liquids.[40] Seddon et al. showed that the sorption properties of water and imidazolium salts depends on the anion,[40] where the sorption capacity was best for the chloride and acetate anions.[41] The cation type is reported to play a minor role on water sorption, which decreases with the increase in length of the alkyl group of the cation.[40,41]

Silica supported ionic liquids maintain the water sorption properties of the pure ionic liquid as it was shown by Askalany et al.,[42] where they measured the isotherms for different degrees of impregnation up to 60 wt% of 1-ethyl-3-methylimidazolium methanesulfonate in Syloid AL-1FP.[42] The sorption isotherms reported by Askalany et al. illustrate that the water uptake of ionogels is more than doubled compared to silica gel.[42] Askalanay et al. further investigated the morphology, water uptake and heat of sorption of two different ionogels.[19] The applicability of ionogel in a sorption desalinator was tested in one experiment at 60 °C showing a very high performance.[19] In addition, Dong et al. investigated their hydrothermal stability.[43]

Ionogels have not been tested in a temperature swing adsorption system below 60 °C.[19] Up until now, no thermal process can be driven by ultra low grade heat at temperatures below 40 °C despite the vast availability of waste heat that is disposed at these temperatures. Therefore, there remains a strong need for novel processes using ultra low temperature waste heat. Ionogels can mitigate thermal pollution by reducing the exergy content of the waste heat flow. Waste heat drives the desorption process and is released during adsorption close to ambient temperature minimising the impact on the environment.

This study fully characterises and tests a novel sorption material on a real sorption desalinator for ultra low grade heat below 40 °C. Materials with such low regeneration temperatures

add a unique feature to adsorption systems, because they allow the utilisation of waste heat that is usually discharged into the environment and cannot be used by any other technology. The vapour-liquid equilibrium of water with a number of commercial ionic liquids have already been measured. Therefore, a preliminary screening of these data identifies the most promising candidates for sorption desalination.

The best ionic liquid is then impregnated in a silica gel support structure and packed into a heat exchanger to assess the performance for regeneration temperatures from 25 °C to 55 °C and different cycle times. The results are compared to other materials presented in the literature to evaluate the competitiveness of the material. To prove the hydrothermal stability of the material, a dynamic vapour sorption experiment measures the isotherms of the ionogel before and after employing it in the test rig, where the material was exposed to vacuum and multiple temperature swings. The entire analysis challenges the applicability of ionogels for sorption desalination in a real device.

Materials and Methods

Adsorption heat transformer

The adsorption heat transformer used for the experimental section features one evaporator, one adsorber and one condenser as shown in Fig. 2. Each vessel is equipped with a heat exchanger, where the adsorber heat exchanger is packed with ionogel. The system is powered by alternatingly cooling the adsorber bed for adsorption and heating the bed for desorption. The evaporating water adsorbs on the ionogel, where the evaporator is slightly heated to increase the relative humidity during adsorption improving the water uptake of the material.[44] After adsorption, the bed is heated, water desorbs and condenses. The condensed water is recirculated to the evaporator, which enables unrestricted experimental run times. The experimental adsorption test rig used for the experiments is presented in Fig. S1 of the Supporting Information and in detail elsewhere.[17,45]

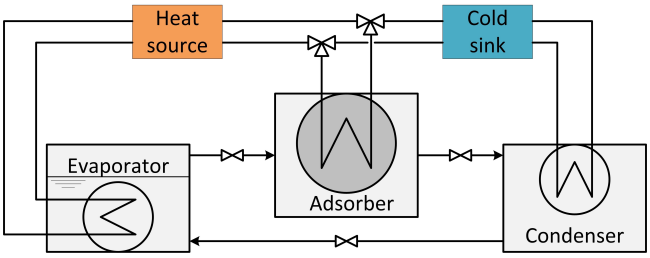

Figure 2: Simplified scheme of the adsorption heat transformer used for the experiments.

Ionic liquid screening

An ionic liquid screening evaluates the working capacities Δq using data from Detherm[46] by plotting the water uptake q [g_w/g_{il}] over the adsorption potential A [kJ/mol] as shown in Fig. 3.

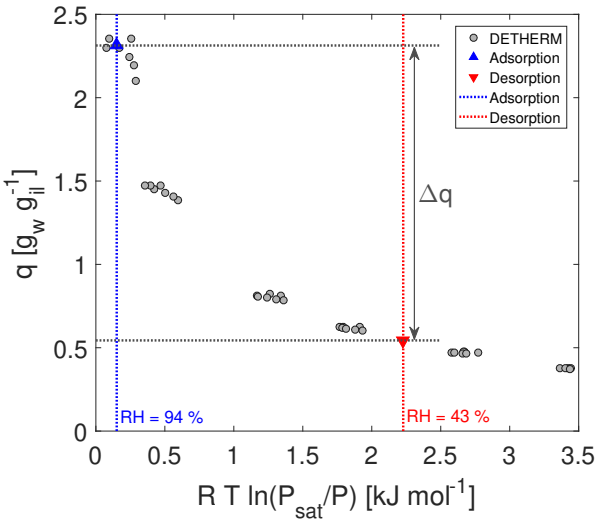

Figure 3: Example evaluation of Δq for 1-ethyl-3-methylimidazolium acetate at T_{evap} = 24 °C, T_{cond} = 25 °C and T_{hot} = 40 °C using DETHERM data from Römrich et al.[47] .

The adsorption potential is given by $A = -RTln(\frac{P}{P_{sat}})$, where R is the universal gas constant[48] [kJ/(molK)], P the absolute vapour pressure [kPa], P_{sat} the saturation pressure of water[48] [kPa] and T the temperature [K]. The uptakes at different temperatures and pressures collapse on a single, characteristic curve when they are plotted over the adsorption potential[49] making the plot temperature independent. The ratio of pressure to saturation

pressure is also referred to as relative humidity $RH = \frac{P}{P_{sat}}$. The investigated temperatures for each vessel are T_{evap} = 22-25 °C, T_{cond} = 25 °C and T_{hot} = 45-50 °C. The results of different working capacities for different RH are listed in table 1. The adsorption potential is calculated for adsorption (0.1-0.5 kJ/mol) and desorption conditions (2-3.5 kJ/mol). For adsorption and desorption, the corresponding water uptake is interpolated from the data. The difference in water uptake between adsorption and desorption equals the working capacity presented in Fig. 3.

Table 1: Working capacities Δq of pure ionic liquids for different relative humidity RH at different $T_{evap,in}$, but constant $T_{cond,in}$ = 25 °C and $T_{hot,in}$ = 50 °C. EMIM = 1-Ethyl-3-methylimidazolium. BMIM = 1-Butyl-3-methylimidazolium. MMIM = 1,3-Dimethylimidazolium. DEP = Diethyl phosphate. DMP = Dimethyl phosphate. SCN = Thiocyanate. TOS = Tosylate. Ac = Acetate. BF_4 = Tetrafluoroborate. ESO_4 = Ethyl sulfate.

RH [%]	83	88	94
Δq	[g_w/g_{il}]	[g_w/g_{il}]	[g_w/g_{il}]
EMIM Ac[47]	1.11	1.62	1.95
EMIM BF_4[50]	0.51	0.86	2.30
EMIM ESO_4[51]	0.88	1.32	2.50
EMIM DEP[52]	1.23	1.65	2.70
BMIM Br[53]	0.58	1.00	2.92
BMIM Cl[54]	1.27	1.74	3.71
BMIM TOS[53]	0.43	0.74	2.18
BMIM Ac[53]	0.95	1.58	2.28
BMIM CH_3SO_3[53]	0.96	1.42	3.22
BMIM CF_3CO_2[53]	0.68	1.18	3.30
BMIM SCN[53]	0.65	1.04	1.75
BMIM CCN[55]	0.43	0.80	2.51
HMIM Cl[54]	0.86	1.53	3.46
MMIM DMP[56]	1.12	1.61	2.74
Siogel silica gel[57]	0.18	0.19	0.21

The ideal ionic liquid should have a large working capacity over a wide range of relative humidity. However, most ionic liquids have a type III adsorption isotherm with water. Less distinct exponential slopes are favourable for the process as they allow a large uptake for a wider range of relative humidity during adsorption. This can also be seen from table 1, where BMIM Br has high working capacities at 94 % relative humidity, but a reduction of

the relative humidity from 94 % to 83 % or T_{evap} by 3 °C has a substantial impact on the uptake. This small temperature change diminishes the working capacity from 2.92 g_w/g_{il} to 0.58 g_w/g_{il}. EMIM Acetate was selected as first ionogel to be tested as it maintains a high working capacity even at lower relative humidity (table 1). In addition, it is a non-hazardous, non-corrosive imidazolium salt.

Preparation

Ionogel was prepared by impregnating Syloid 72FP (W.R. Grace, USA) with EMIM Ac (97 % purity, Sigma Aldrich, USA) achieving a mass proportion of Syoloid 72FP/EMIM Ac 43 wt%/57 wt%. Afterwards, one heat exchanger was prepared and weighed as follows: drying of the heat exchanger; filling it with ionogel by compacting it in monoliths in between the fins; drying the ionogel inside the heat exchanger at 80 °C.

The ionogel inside the heat exchanger was aged to minimise the leakage of ionic liquid inside the test rig.[43] The ageing process included adsorption of water for 40 h at high humidity and ambient conditions and water desorption from the ionogel inside the heat exchanger at 80 °C. The heat exchanger was filled with 25.1 g of ionogel with an EMIM Ac content of 57 wt% for the experiments in the test rig. The amount of ionogel was reduced to 25.1 g to limit the total amount of water evaporating during a cycle to achieve a more homogeneous temperature distribution in the evaporator.

Results and discussion

Material analysis

Scanning electron microscope images (ZEISS Crossbeam 550 Cryo FIB/SEM) were taken before testing the ionogel in the adsorption desalinator and are presented in Fig. 4 as well as Fig. S1, Supporting Information. Syloid 72FP has an average particle size of 4.6-5.8 μm,[58] while the average pore diameter of Syloid 72FP silica gel is 10-15 nm,[59,60] which is shown in

Fig. 4a. The particles have a large size distribution forming agglomerates without regular structure. The silica gel particles are supporting the ionogel with the ionic liquid coating the surface, partially filling the pores and acting as binder at the same time. The ionic liquid fills the pores and coats the external surface of the silica gel particles in Fig. 4b. Focus ion beam *FIB* etching was applied to view inside an ionogel particle in Fig 4c, where the particle maintains some pores below a few hundred nanometre thick surface coating of EMIM Ac. This surface layer of ionic liquid in Fig. 4b obstructs the porous structure of silica gel causing water vapour to interact with the electrical charges of the ionic liquid instead of the pores.

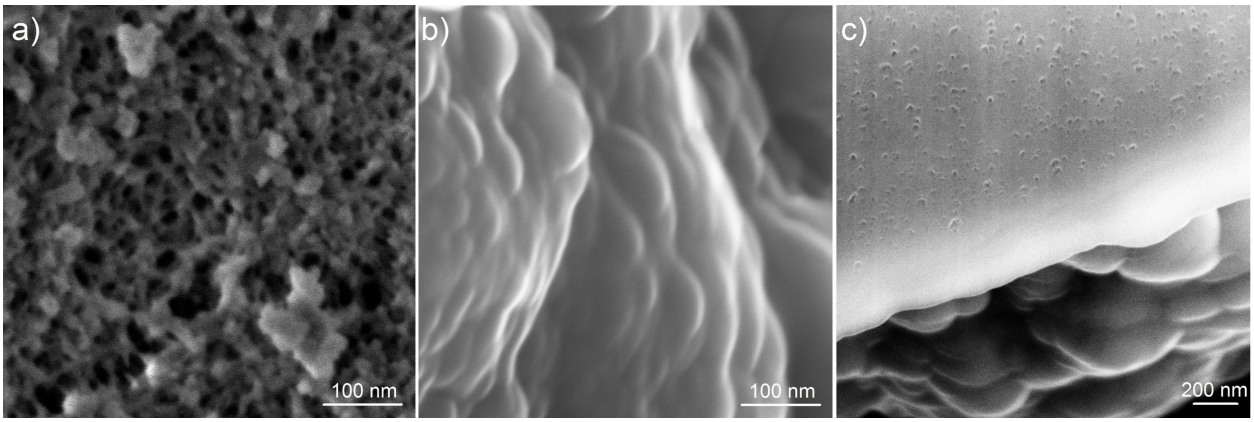

Figure 4: (a) Pure Syloid 72FP silica gel: The open pore structure is visible with pore sizes averaging between 10-15 nm.[59,60] (SEM image)
(b) Ionogel: EMIM Ac coats the surface of Syloid 72FP silica gel. (SEM image of the material after cycling)
(c) Ionogel: SEM image of FIB etched particle shows that the porous structure is partially filled below the surface. The image shows the cycled ionogel.

This is confirmed by Energy Dispersive Spectroscopy *EDS* of a FIB etched particle in Fig. 5. An SEM image of the same FIB etched particle is shown in Fig. 1f, SI. The EDS analysis focused on Carbon for EMIM Ac ($C_8H_{14}N_2O_2$) and Silicon for silica gel (SiO_2), which are only present in each one of the components. The ionic liquid mainly appears on the particle surface and directly below the surface, whereas the carbon distribution is low in the core of the particle.

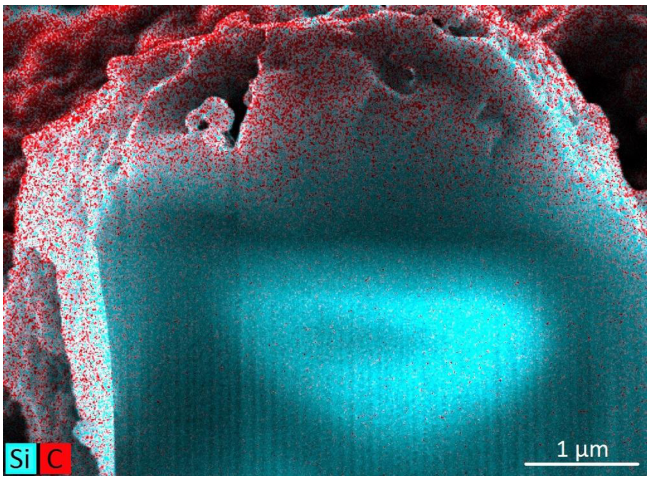

Figure 5: EDS image of FIB etched Ionogel particle. Silicon represents silica gel and Carbon for EMIM Ac. The spectral data is provided in Fig. S2, Supporting Information.

Fig. 6a displays the material after exposing it to several hundred temperature swings, which causes material ageing. Before the experiments, ionogel is a white, dull, brittle substance that turns into a grey, glossy gel due to water uptake (Fig. 6a). The colour shifts back to white, when the material is dried. Isotherms were measured using dynamic vapour sorption (DVS Adventure, Surface Measurement Systems Ltd., UK) to analyse the material stability. Fig. 6b shows the adsorption isotherm of the fresh, not cycled material as well as the isotherm of the cycled ionogel for adsorption and desorption. The data points of the fresh and cycled material overlap highlighting the material stability. In addition, Ionogel does not have a hysteresis as the data for adsorption and desorption overlaps. This feature results in higher performance when used in real temperature swing devices. The Dubinin-Astakhov[49,61] equation $q = q_0\ exp[-(\frac{RT}{E}\ ln(\frac{P_{sat}}{P}))^n]$ was used to fit the isotherm with the DA fitting parameters q_0, E and n given in table 2. The heat of sorption is reported by Askalany et al. and is essentially equal to the latent heat of water over a wide range of water uptakes.[19]

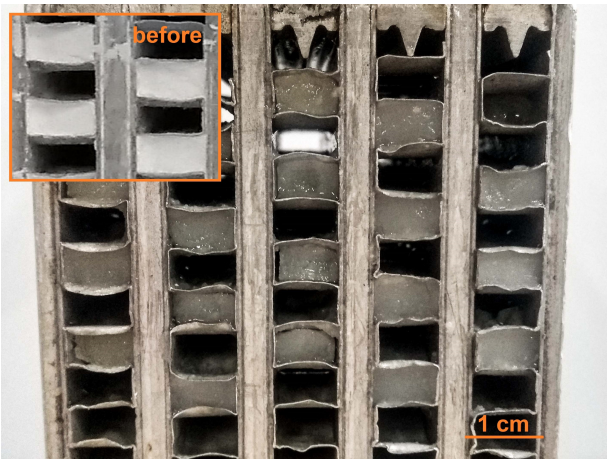

(a)

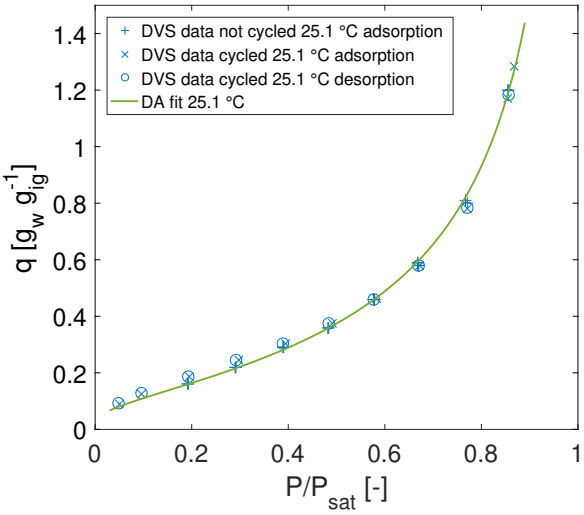

(b)

Figure 6: (a) The fresh material is a white, brittle, powdery substance, whereas cycling turns it grey and shimmering.
(b) Measured isotherm of the cycled and the not cycled material, which are both fitted (from tables S1 and S2, Supporting Information) to the Dubinin-Astakhov isotherm equation (table 2).

Raman spectra (Fig. S4 and Fig. S5, Supporting Information) from 5 °C to 80 °C confirm the thermal stability of the ionogel and show the material composition at different degrees of EMIM Ac impregnation. Additional research is required to identify a combination of ionic liquid and support material to achieve the same performance at lower relative humidity. This would further improve the performance in desalination, but also allow the application in air conditioning or refrigeration.

Table 2: Dubinin-Astakhov parameters for Syloid 72FP impregnated with 57 wt% EMIM Ac ionogel

	q_0 [g_w/g_{ig}]	E [J/mol]	n [-]
Ionogel	32.2	1.04	0.20

Performance

A full characterisation of the novel ionogel material was conducted inside the adsorption desalinator aiming at identifying the minimum regeneration temperature, optimal cycle time

and the performance of the material when integrated within a real device. The test rig was operated in one bed mode adsorbing at 20 °C and desorbing at different temperatures from 25 °C to 55 °C increased in increments of 5 °C for each experiment. The evaporator inlet temperature $T_{evap,in}$ was adjusted so that the vapour temperature $T_{evap,vap}<T_{ads,in}$ and $T_{evap} \approx T_{cond} \approx 20$ °C for all ionogel experiments. This condition assures that the water vapour during adsorption is colder than the heat exchanger surface to prevent condensation. The driving temperature difference powering the process is therefore $\Delta T = T_{hot} - T_{cond}$ as given in Fig. 7.

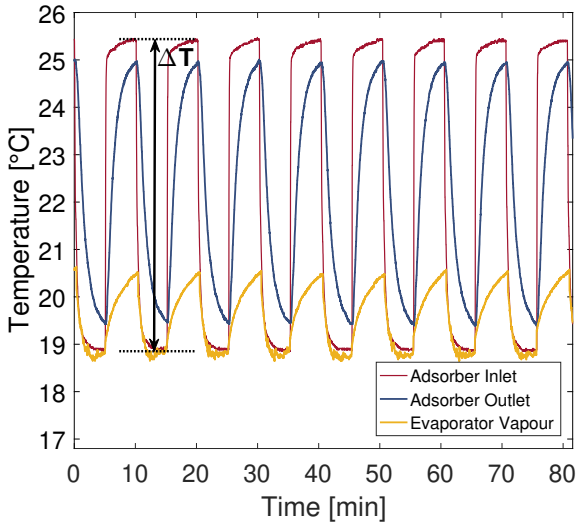

Figure 7: Temperature curves obtained from experiment at $\Delta T \approx 5$ °C, $T_{cond,in} = 20$ °C, $T_{hot,in} = 25$ °C and 280 s half cycle time.

Fig. 7 shows the temperature swings at the unprecedented ultra-low regeneration temperature of $T_{hot,in} = 25$ °C, where the process is operated within $\Delta T \approx 5$ °C. No other adsorption material can be regenerated at such low temperature differences. It can be seen that $T_{evap,vap} < T_{ads,in}$ was maintained at all times to avoid condensation. The temperature increase between inlet and outlet of 1 °C has to be attributed to the removal of the remaining sensible heat in the aluminium heat exchanger as the contribution of the heat of adsorption is very small less than 0.1 °C. The water production during the experiment in Fig. 7 reaches a peak value of 0.4 g/min, which decreases at the end of desorption to less than 0.1 g/min

(Fig. S3,Supporting Information).

Seven different hot temperatures have been investigated in the same way to assess the Specific Daily Water Production SDWP of the material: $SDWP = N_c \int_0^{t_c} \frac{\dot{Q}_{cond}}{L_w \cdot M_{ig}} dt$, where N_c is the number of cycles per day [-], $\dot{Q}_{cond}$ the condenser heat [kW], t_c the cycle time [s], L_w the latent heat of water [kJ/kg] and M_{ig} the mass of ionogel [kg]. The ionogel results are compared to silica gel (Siogel, microporous beads 0.5-2 mm Oker Chemie GmbH, Germany) using the same aluminium heat exchangers in both cases.[17,45] The silica gel experiments were conducted using 210 g per adsorber in two-bed mode and are reported in a previous study.[17] The analysis in Fig 8a investigates the optimal half cycle time to achieve the highest SDWP, which is an important preliminary step for the study on the heat source temperature in Fig. 8b. The SDWP is highest for half cycle times of 180 s to 300 s. Thus, half cycles of 240 s were chosen for the experiments at different low temperatures. Silica gel requires much longer half cycle times of 600 s to 1200 s. The heat transfer of the ionogel monoliths is improved as they share a larger surface area with the aluminium heat exchanger than the silica gel beads. Ionogel has higher adsorption rates, where it reaches the same working capacity as silica gel in a quarter of the time. However, the working capacities of ionogel in this set of experiments remained well below the working capacities suggested by the isotherms. In the test rig, the working capacities were around 0.2 g_w/g_{ig}, while the isotherms predict $\Delta q > 1$ g_w/g_{ig}. The deviation of the two Δq correspond to Cao et al.,[41] who reported fast sorption kinetics at first, which slow down at higher water uptakes. The isotherms illustrate the water uptake at equilibrium, while the material cannot reach equilibrium within useful half cycles times in the test rig. Hence, the high SDWP of ionogel are a result of the fast kinetics and improved heat and mass transfer compared to silica gel, but not due to the large Δq at equilibrium.

Fig. 8b shows the resulting SDWP for each hot temperature and compares them to experimental results of silica gel measured in the same test rig.[17] The results are plotted over ΔT to allow a comparison. Both materials show an almost linear increase of the SDWP

at low temperatures until they reach a plateau, which begins at $\Delta T \approx 25$ °C for ionogel and $\Delta T \approx 30$ °C for silica gel. The maximum SDWP of ionogel is 17.5 $kg_w/(kg_{ig}d)$, which is almost double the SDWP of silica gel at 10.9 $kg_w/(kg_{sg}d)$. However, ionogel does not have a minimum regeneration temperature, because even at $\Delta T = 5$ °C it achieves SDWP = 6.7 $kg_w/(kg_{ig}d)$, which is comparable to the best silica gel results. By contrast, silica gel needs a temperature difference of at least 15 °C for SDWP = 2.8 $kg_w/(kg_{sg}d)$, where ionogel is four times better achieving SDWP = 11.3 $kg_w/(kg_{ig}d)$ at $\Delta T = 15$ °C.

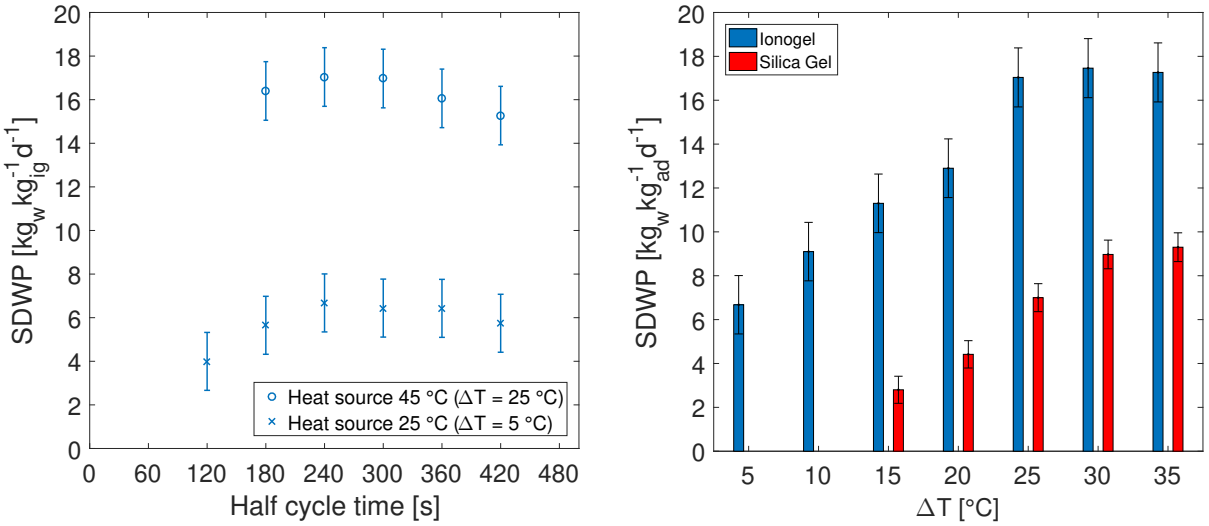

(a) (b)

Figure 8: (a) Experimental cycle time analysis for ionogel at $T_{cond} = 20$ °C.
(b) Experimental SDWP comparison of silica gel and ionogel for different $\Delta T = T_{hot} - T_{cond}$. Ionogel: $T_{cond} = 20$ °C half cycle time 240 s. Silica gel: $T_{cond} = 25$ °C half cycle time 1200 s.

The experimental results are compared to recent, experimental studies in adsorption desalination in Fig. 9.[18,62–64] The results highlight the unrivalled features of ionogels compared to materials tested in other systems. Thu et al. have presented a 4 bed system with silica gel, which is currently the largest system and best performing system using silica gel.[18] In a study from 2011 they reported the highest SDWP using their 4 bed system and silica gel achieving 14.2 $kg_w/(kg_{sg}d)$ with $\Delta T = 55$ °C.[65] The highest SDWP in their recent study is SDWP = 11 $kg_w/(kg_{sg}d)$ at $\Delta T = 45$ °C.[18] Youssef et al. investigated the application of

CPO27Ni MOF-material, which achieves high performances similar to ionogel.[63] However, the regeneration temperatures are at least 95 °C or $\Delta T = 80$ °C, while ionogel achieves a higher SDWP than CPO27Ni at $\Delta T = 25$ °C. Fig. 9 also shows the highest SDWP achieved with the experimental apparatus of this study and silica gel.[17] Even at $\Delta T = 50$ °C silica gel can only reach SDWP = 10.9 $kg_w/(kg_{sg}d)$ in the same test rig,[17] which is less than ionogel at $\Delta T = 15$ °C in Fig. 8b. Hence, the material features outstanding properties for water desalination applications driven by very low heat source temperatures, but the material also shows great potential for thermal energy storage as well as sorption cooling applications.

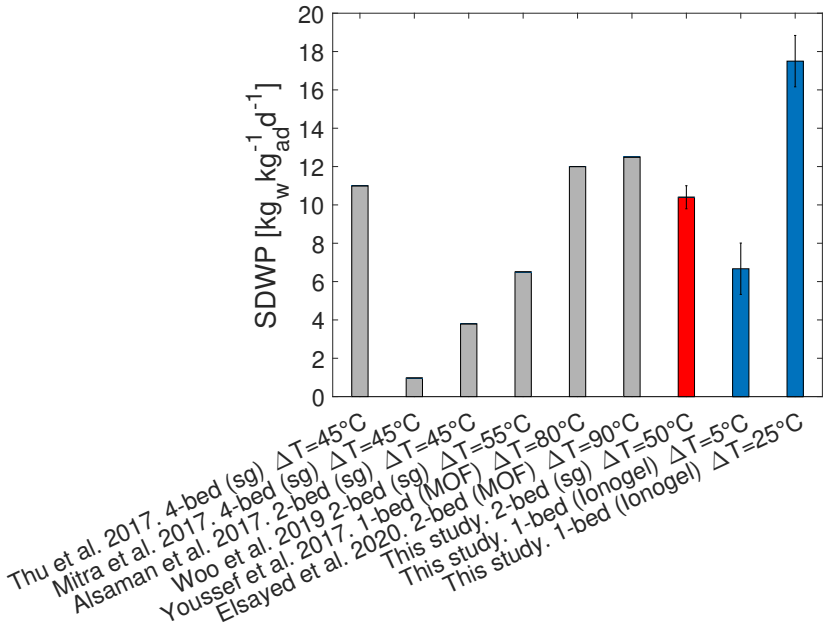

Figure 9: Comparison of ionogel to other studies and materials[18,33,62–64,66]

Associated content

Supporting Information is available: Photo and description of the experimental adsorption desalinator. Six additional SEM images showing the material surface and further FIB etching results. EDS map sum spectra of the FIB etched ionogel particle. Water production curves calculated from Fig. 7. Two Raman spectra at different ionic liquid impregnation proportions

and temperatures. Two tables of experimental isotherm data of the cycled and not cycled ionogel material.

Acknowledgements

This work was funded by the Horizon 2020 programme (RED-Heat-to-Power project: Conversion of Low-grade Heat to Power through closed loop Reverse Electro-Dialysis. Project number: 640667) and the EPSRC (Micro-scale energy storage for super-efficient wet appliances. Project number: EP/P010954/1). Moreover, we acknowledge the use of the Cryo FIB/SEM bought with the EPSRC grant EP/P030564/1 and Thomas Glen for support with image acquisition.

References

(1) Raptis, C. E.; van Vliet, M. T. H.; Pfister, S. Global thermal pollution of rivers from thermoelectric power plants. *Environ. Res. Lett.* **2016**, *11*, 104011.

(2) Verones, F.; Hanafiah, M. M.; Pfister, S.; Huijbregts, M. A. J.; Pelletier, G. J.; Koehler, A. Characterization Factors for Thermal Pollution in Freshwater Aquatic Environments. *Environ. Sci. Technol.* **2010**, *44*, 9364–9369.

(3) Jacobson, M. Z. Review of solutions to global warming, air pollution, and energy security. *Energy Environ. Sci.* **2009**, *2*, 148–173.

(4) Forman, C.; Muritala, I. K.; Pardemann, R.; Meyer, B. Estimating the global waste heat potential. *Renew. Sustain. Energy Rev.* **2016**, *57*, 1568–1579.

(5) Rattner, A. S.; Garimella, S. Energy harvesting, reuse and upgrade to reduce primary energy usage in the USA. *Energy* **2011**, *36*, 6172 – 6183.

(6) Van Vliet, M. T.; Yearsley, J. R.; Ludwig, F.; Vögele, S.; Lettenmaier, D. P.; Kabat, P. Vulnerability of US and European electricity supply to climate change. *Nat. Clim. Change* **2012**, *2*, 676.

(7) Walker, M. E.; Lv, Z.; Masanet, E. Industrial Steam Systems and the Energy-Water Nexus. *Environ. Sci. Technol.* **2013**, *47*, 13060–13067.

(8) Davidson, B.; Bradshaw, R. W. Thermal Pollution of Water Systems. *Environ. Sci. Technol.* **1967**, *1*, 618–630.

(9) Quijano, J. C.; Jackson, P. R.; Santacruz, S.; Morales, V. M.; García, M. H. Implications of Climate Change on the Heat Budget of Lentic Systems Used for Power Station Cooling: Case Study Clinton Lake, Illinois. *Environ. Sci. Technol.* **2016**, *50*, 478–488.

(10) Sanders, K. T. Critical Review: Uncharted Waters? The Future of the Electricity-Water Nexus. *Environ. Sci. Technol.* **2015**, *49*, 51–66.

(11) Rosen, M. A. Energy- and exergy-based comparison of coal-fired and nuclear steam power plants. *Int. J. Exergy* **2001**, *1*, 180 – 192.

(12) Li, C.; Goswami, Y.; Stefanakos, E. Solar assisted sea water desalination: A review. *Renew. Sustain. Energy Rev.* **2013**, *19*, 136 – 163.

(13) Carballo, J. A.; Bonilla, J.; Roca, L.; la Calle, A. D.; Palenzuela, P.; Alarcón-Padilla, D. C. Optimal operating conditions analysis for a multi-effect distillation plant according to energetic and exergetic criteria. *Desalination* **2018**, *435*, 70 – 76, Desalination using Renewable Energy.

(14) Chang, Z.; Zheng, H.; Yang, Y.; Su, Y.; Duan, Z. Experimental investigation of a novel multi-effect solar desalination system based on humidification–dehumidification process. *Renew. Energy Rev.* **2014**, *69*, 253 – 259.

(15) Zaragoza, G.; Ruiz-Aguirre, A.; Guillén-Burrieza, E. Efficiency in the use of solar thermal energy of small membrane desalination systems for decentralized water production. *Appl. Energy* **2014**, *130*, 491 – 499.

(16) Dow, N.; Gray, S.; de Li, J.; Zhang, J.; Ostarcevic, E.; Liubinas, A.; Atherton, P.; Roeszler, G.; Gibbs, A.; Duke, M. Pilot trial of membrane distillation driven by low grade waste heat: Membrane fouling and energy assessment. *Desalination* **2016**, *391*, 30 – 42, Advances in Membrane Des: Keynotes from MEMDES 2-Singapore.

(17) Olkis, C.; Brandani, S.; Santori, G. Cycle and performance analysis of a small-scale adsorption heat transformer for desalination and cooling applications. *Chem. Eng. J.* **2019**, *378*, 122104.

(18) Thu, K.; Yanagi, H.; Saha, B. B.; Ng, K. C. Performance investigation on a 4-bed adsorption desalination cycle with internal heat recovery scheme. *Desalination* **2017**, *402*, 88 – 96.

(19) Askalany, A.; Olkis, C.; Bramanti, E.; Lapshin, D.; Calabrese, L.; Proverbio, E.; Freni, A.; Santori, G. Silica-Supported Ionic Liquids for Heat-Powered Sorption Desalination. *ACS Appl. Mater. Interfaces* **2019**, *11*, 36497–36505.

(20) Rahimi, M.; Straub, A. P.; Zhang, F.; Zhu, X.; Elimelech, M.; Gorski, C. A.; Logan, B. E. Emerging electrochemical and membrane-based systems to convert low-grade heat to electricity. *Energy Environ. Sci.* **2018**, *11*, 276–285.

(21) Zhang, F.; Liu, J.; Yang, W.; Logan, B. E. A thermally regenerative ammonia-based battery for efficient harvesting of low-grade thermal energy as electrical power. *Energy Environ. Sci.* **2015**, *8*, 343–349.

(22) Shengjun, Z.; Huaixin, W.; Tao, G. Performance comparison and parametric optimization of subcritical Organic Rankine Cycle (ORC) and transcritical power cycle system for low-temperature geothermal power generation. *Appl. Energy* **2011**, *88*, 2740 – 2754.

(23) Yip, N. Y.; Elimelech, M. Thermodynamic and energy efficiency analysis of power generation from natural salinity gradients by pressure retarded osmosis. *Environ. Sci. Technol.* **2012**, *46*, 5230–5239.

(24) Tamburini, A.; Tedesco, M.; Cipollina, A.; Micale, G.; Ciofalo, M.; Papapetrou, M.; Baak, W. V.; Piacentino, A. Reverse electrodialysis heat engine for sustainable power production. *Appl. Energy* **2017**, *206*, 1334 – 1353.

(25) Giacalone, F.; Olkis, C.; Santori, G.; Cipollina, A.; Brandani, S.; Micale, G. Novel solutions for closed-loop reverse electrodialysis: Thermodynamic characterisation and perspective analysis. *Energy* **2019**, *166*, 674 – 689.

(26) Logan, B. E.; Elimelech, M. Membrane-based processes for sustainable power generation using water. *Nature* **2012**, *488*, 313.

(27) Rijnaarts, T.; Huerta, E.; van Baak, W.; Nijmeijer, K. Effect of Divalent Cations on RED Performance and Cation Exchange Membrane Selection to Enhance Power Densities. *Environ. Sci. Technol.* **2017**, *51*, 13028–13035.

(28) Lin, S.; Yip, N. Y.; Cath, T. Y.; Osuji, C. O.; Elimelech, M. Hybrid pressure retarded osmosis–membrane distillation system for power generation from low-grade heat: Thermodynamic analysis and energy efficiency. *Environ. Sci. Technol.* **2014**, *48*, 5306–5313.

(29) Olkis, C.; Santori, G.; Brandani, S. An Adsorption Reverse Electrodialysis system for the generation of electricity from low-grade heat. *Appl. Energy* **2018**, *231*, 222 – 234.

(30) Ng, K. C.; Thu, K.; Kim, Y.; Chakraborty, A.; Amy, G. Adsorption desalination: An emerging low-cost thermal desalination method. *Desalination* **2013**, *308*, 161 – 179, New Directions in Desalination.

(31) Sapienza, A.; Gullì, G.; Calabrese, L.; Palomba, V.; Frazzica, A.; Brancato, V.; Rosa, D. L.; Vasta, S.; Freni, A.; Bonaccorsi, L.; Cacciola, G. An innovative adsorptive

chiller prototype based on 3 hybrid coated/granular adsorbers. *Appl. Energy* **2016**, *179*, 929 – 938.

(32) Grabowska, K.; Krzywanski, J.; Nowak, W.; Wesolowska, M. Construction of an innovative adsorbent bed configuration in the adsorption chiller - Selection criteria for effective sorbent-glue pair. *Energy* **2018**, *151*, 317 – 323.

(33) Woo, S.-Y.; Lee, H.-S.; Ji, H.; Moon, D.-S.; Kim, Y.-D. Silica gel-based adsorption cooling cum desalination system: Focus on brine salinity, operating pressure, and its effect on performance. *Desalination* **2019**, *467*, 136 – 146.

(34) de Lange, M. F.; Verouden, K. J. F. M.; Vlugt, T. J. H.; Gascon, J.; Kapteijn, F. Adsorption-Driven Heat Pumps: The Potential of Metal–Organic Frameworks. *Chem. Rev.* **2015**, *115*, 12205–12250.

(35) Elsayed, E.; AL-Dadah, R.; Mahmoud, S.; Anderson, P.; Elsayed, A.; Youssef, P. G. CPO-27(Ni), aluminium fumarate and MIL-101(Cr) MOF materials for adsorption water desalination. *Desalination* **2017**, *406*, 25 – 36, Desalination and the Environment.

(36) Canivet, J.; Fateeva, A.; Guo, Y.; Coasne, B.; Farrusseng, D. Water adsorption in MOFs: fundamentals and applications. *Chem. Soc. Rev.* **2014**, *43*, 5594–5617.

(37) Wishart, J. F. Energy applications of ionic liquids. *Energy Environ. Sci.* **2009**, *2*, 956–961.

(38) Le Bideau, J.; Viau, L.; Vioux, A. Ionogels, ionic liquid based hybrid materials. *Chem. Soc. Rev.* **2011**, *40*, 907–925.

(39) Pal, A.; Shahrom, M. S. R.; Moniruzzaman, M.; Wilfred, C. D.; Mitra, S.; Thu, K.; Saha, B. B. Ionic liquid as a new binder for activated carbon based consolidated composite adsorbents. *Chem. Eng. J.* **2017**, *326*, 980 – 986.

(40) Seddon, K. R.; Stark, A.; Torres, M.-J. Influence of chloride, water, and organic solvents on the physical properties of ionic liquids. *Pure Appl. Chem.* **2000**, *72*, 2275–2287.

(41) Cao, Y.; Chen, Y.; Sun, X.; Zhang, Z.; Mu, T. Water sorption in ionic liquids: kinetics, mechanisms and hydrophilicity. *Phys. Chem. Chem. Phys.* **2012**, *14*, 12252–12262.

(42) Askalany, A. A.; Freni, A.; Santori, G. Supported ionic liquid water sorbent for high throughput desalination and drying. *Desalination* **2019**, *452*, 258 – 264.

(43) Dong, H.; Askalany, A. A.; Olkis, C.; Zhao, J.; Santori, G. Hydrothermal stability of water sorption ionogels. *Energy* **2019**, *189*, 116186.

(44) Wu, J. W.; Hu, E. J.; Biggs, M. J. Thermodynamic cycles of adsorption desalination system. *Appl. Energy* **2012**, *90*, 316–322.

(45) Olkis, C.; Brandani, S.; Santori, G. Design and experimental study of a small scale adsorption desalinator. *Appl. Energy* **2019**, *253*, 113584.

(46) Westhaus, U.; Dröge, T.; Sass, R. DETHERM®—a thermophysical property database. *Fluid Ph. Equilibria* **1999**, *158-160*, 429 – 435.

(47) Roemich, C.; Merkel, N. C.; Valbonesi, A.; Schaber, K.; Sauer, S.; Schubert, T. J. Thermodynamic properties of binary mixtures of water and room-temperature ionic liquids: Vapor pressures, heat capacities, densities, and viscosities of water+ 1-ethyl-3-methylimidazolium acetate and water+ diethylmethylammonium methane sulfonate. *J. Chem. Eng. Data* **2012**, *57*, 2258–2264.

(48) Verein deutscher Ingenieure, In *VDI-Wärmeatlas*, 11th ed.; VDI e.V.,, Ed.; VDI-Buch; Springer: Berlin Heidelberg, 2013.

(49) Dubinin, M. M.; Astakhov, V. A. Development of the concepts of volume filling of micropores in the adsorption of gases and vapors by microporous adsorbents. *Bull. USSR Acad. Sci.* **1971**, *20*, 3–7.

(50) Jork, C.; Seiler, M.; Beste, Y.-A.; Arlt, W. Influence of ionic liquids on the phase behavior of aqueous azeotropic systems. *J. Chem. Eng. Data* **2004**, *49*, 852–857.

(51) Calvar, N.; Gonzalez, B.; Gomez, E.; Dominguez, A. Vapor–liquid equilibria for the ternary system ethanol+ water+ 1-ethyl-3-methylimidazolium ethylsulfate and the corresponding binary systems containing the ionic liquid at 101.3 kPa. *J. Chem. Eng. Data* **2008**, *53*, 820–825.

(52) Peng, Y.; Lu, X. Isobaric Vapor–Liquid Equilibria for Water + Acetic Acid + 1-Ethyl-3-methylimidazolium Diethylphosphate at 101.32 kPa. *J. Chem. Eng. Data* **2014**, *59*, 250–256.

(53) Passos, H.; Khan, I.; Mutelet, F.; Oliveira, M. B.; Carvalho, P. J.; Santos, L. M.; Held, C.; Sadowski, G.; Freire, M. G.; Coutinho, J. A. Vapor–Liquid Equilibria of Water+ Alkylimidazolium-Based Ionic Liquids: Measurements and Perturbed-Chain Statistical Associating Fluid Theory Modeling. *Ind. Eng. Chem. Res.* **2014**, *53*, 3737–3748.

(54) Carvalho, P. J.; Khan, I.; Morais, A.; Granjo, J. F.; Oliveira, N. M.; Santos, L. M.; Coutinho, J. A. A new microebulliometer for the measurement of the vapor–liquid equilibrium of ionic liquid systems. *Fluid Ph. Equilibria* **2013**, *354*, 156–165.

(55) Huang, Y.; Zhang, X.; Zhang, X.; Dong, H.; Zhang, S. Thermodynamic Modeling and Assessment of Ionic Liquid-Based CO2 Capture Processes. *Ind. Eng. Chem. Res.* **2014**, *53*, 11805–11817.

(56) Kato, R.; Gmehling, J. Measurement and correlation of vapor–liquid equilibria of binary systems containing the ionic liquids [EMIM][(CF 3 SO 2) 2 N],[BMIM][(CF 3 SO 2) 2 N],[MMIM][(CH 3) 2 PO 4] and oxygenated organic compounds respectively water. *Fluid Ph. Equilibria* **2005**, *231*, 38–43.

(57) Sapienza, A.; Velte, A.; Girnik, I.; Frazzica, A.; Füldner, G.; Schnabel, L.; Aristov, Y. "Water - Silica Siogel" working pair for adsorption chillers: Adsorption equilibrium and dynamics. *Renew. Energy Rev.* **2017**, *110*, 40 – 46.

(58) Hussain, T.; Waters, L. J.; Parkes, G. M.; Shahzad, Y. Microwave processed solid dispersions for enhanced dissolution of gemfibrozil using non-ordered mesoporous silica. *Colloids Surf., A* **2017**, *520*, 428 – 435.

(59) Hespeler, D.; Kaltenbach, J.; Pyo, S. M. Glabridin smartPearls – Silica selection, production, amorphous stability and enhanced solubility. *Int. J. Pharm.* **2019**, *561*, 228 – 235.

(60) Weerapol, Y.; Limmatvapirat, S.; Jansakul, C.; Takeuchi, H.; Sriamornsak, P. Enhanced dissolution and oral bioavailability of nifedipine by spontaneous emulsifying powders: Effect of solid carriers and dietary state. *Eur. J. Pharm. Biopharm.* **2015**, *91*, 25 – 34.

(61) Santori, G.; Santis, C. D. Optimal fluids for adsorptive cooling and heating. *Sustain. Mat. Technol.* **2017**, *12*, 52 – 61.

(62) Mitra, S.; Thu, K.; Saha, B. B.; Dutta, P. Performance evaluation and determination of minimum desorption temperature of a two-stage air cooled silica gel/water adsorption system. *Appl. Energy* **2017**, *206*, 507 – 518.

(63) Youssef, P. G.; Dakkama, H.; Mahmoud, S. M.; AL-Dadah, R. K. Experimental investigation of adsorption water desalination/cooling system using CPO-27Ni MOF. *Desalination* **2017**, *404*, 192–199.

(64) Alsaman, A. S.; Askalany, A. A.; Harby, K.; Ahmed, M. S. Performance evaluation of a solar-driven adsorption desalination-cooling system. *Energy* **2017**, *128*, 196 – 207.

(65) Thu, K.; Saha, B. B.; Chakraborty, A.; Chun, W. G.; Ng, K. C. Study on an advanced

adsorption desalination cycle with evaporator–condenser heat recovery circuit. *Int. J. Heat Mass Transf.* **2011**, *54*, 43–51.

(66) Elsayed, E.; AL-Dadah, R.; Mahmoud, S.; Anderson, P.; Elsayed, A. Experimental testing of aluminium fumarate MOF for adsorption desalination. *Desalination* **2020**, *475*, 114170.